A&A 506, 955–964 (2009)
DOI: 10.1051/0004-6361/200912371
© ESO 2009

Astronomy & Astrophysics

Ionization processes in the atmosphere of Titan

I. Ionization in the whole atmosphere

G. Gronoff[1], J. Lilensten[1], L. Desorgher[2,3], and E. Flückiger[2]

[1] Laboratoire de Planétologie de Grenoble, Université Joseph Fourier - CNRS, France
e-mail: guillaume.gronoff@obs.ujf-grenoble.fr
[2] Physikalisches Institut, University of Bern, Switzerland
[3] SpaceIT GmbH, Sennweg 15, 3012 Bern, Switzerland

Received 22 April 2009 / Accepted 13 July 2009

ABSTRACT

Context. The Cassini probe regularly passes in the vicinity of Titan, revealing new insights into particle precipitation thanks to the electron and proton spectrometer. Moreover, the Huygens probe has revealed an ionized layer at 65 km induced by cosmic rays. The impact of these different particles on the chemistry of Titan is probably very strong.
Aims. In this article, we compute the whole ionization in the atmosphere of Titan: from the cosmic rays near the ground to the EUV in the upper atmosphere. The meteoritic layer is not taken into account.
Methods. We used the transTitan model to compute the electron and EUV impact, and the planetocosmics code to compute the influence of protons and oxygen ions. We coupled the two models to study the influence of the secondary electrons obtained by planetocosmics through the transTitan code. The resulting model improves the accuracy of the calculation through the transport of electrons in the atmosphere.
Results. The whole ionization is computed and studied in details. During the day, the cosmic ray ionization peak is as strong as the UV-EUV one. Electrons and protons are very important depending the precipitation conditions. Protons can create a layer at 500 km, while electrons tend to ionize near 800 km. The oxygen ion impact is near 900 km. The results shows few differences to precedent models for the nightside T5 fly-by of Cassini, and can highlight the sources of the different ion layers detected by radio measurements.
Conclusions. The new model successfully computes the ion production in the atmosphere of Titan. For the first time, a full electron and ion profile has been computed from 0 to 1600 km, which compares qualitatively with measurements. This result can be used by chemical models.

Key words. planets and satellites: individual: Titan – atmospheric effects – Sun: UV radiation – space vehicles: instruments – methods: numerical

1. Introduction

Solar EUV – XUV radiation, energetic plasma from Saturn's magnetosphere, and cosmic rays are the main sources of the ionization of the neutral gas in Titan's atmosphere. Each source has a main ionization altitude that creates several ionosphere layers above 50 km (Cravens et al. 2008, 2009; Hamelin et al. 2007; López-Moreno et al. 2008, and references therein). While Titan can be inside or outside of the Saturn's magnetosphere, particle precipitation, hence ionization can be very variable depending on the position of the satellite and local plasma conditions. Knowledge of the whole ionization profile in the atmosphere of Titan is however widespread, although the formation of the large atmospheric molecules at all altitudes, including in the detached haze (at about 500 km) remains poorly understood and could depend on ion – neutral chemistry. The present paper and its second part, "Electron precipitation along magnetic field lines" (Gronoff et al. 2009), presents the results of the transTitan-planetocosmics models, which is now able to compute this whole ionization. The chemistry is beyond the scope of these papers, but computing ion and electron production, addressed here, is necessary. In the present paper, we compare the results of the coupled model transTitan-planetocosmics with the different observations from Cassini and Huygens probes. It allows the different ionospheric layers to be interpreted in terms of precipitating sources: UV and electron in the upper atmosphere, protons in the middle atmosphere (500 km), and cosmic rays in the lower atmosphere (peak at 65 km). In the second paper, we study the electron impact ionization in detail, which strongly depends on the geometry of magnetic field, by comparing it to Cassini measurements.

2. The energetic sources in Titan's atmosphere

The aim of this paper is to compute those ionization and excitation rates in Titan's atmosphere that come from energetic sources. These are the EUV/XUV flux, the electron and proton precipitations, the cosmic rays, and, to a lesser extend, ion precipitations (Fig. 1). The meteoritic source is neglected in this study.

2.1. The EUV/XUV source

Different categories of aeronomical models have been used in the past for modeling the primary EUV/XUV flux. The first one consists of models that were first developed in the eighties and that rely heavily on data from Atmospheric Explorer mission (Hinteregger et al. 1973). Many models today still use the binning of the spectrum that was first proposed by Torr et al. (1979). The success of this approach has to do with its simplicity

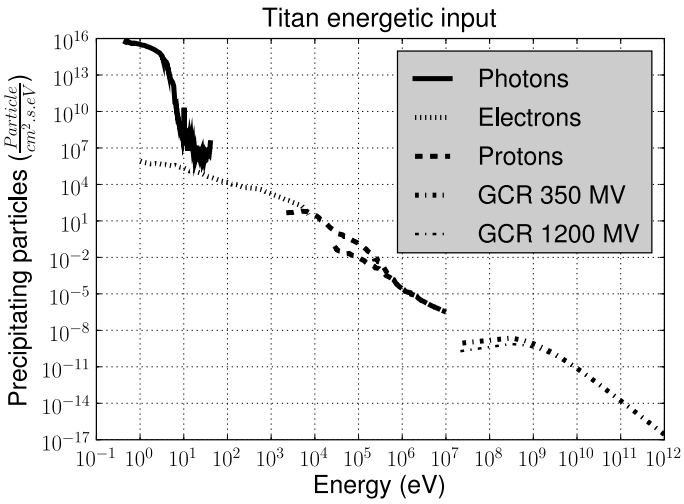

Fig. 1. The energetic input into the atmosphere of Titan.

and the set of absorption cross sections for each wavelength bin. There are two reference fluxes: one for solar-active and one for solar-quiet conditions. Other levels of activity are modeled by interpolating the decimetric index $F_{10.7}$. The experimental data used to determine the flux has gradually improved since then (Hinteregger 1981; Hinteregger et al. 1981; Torr & Torr 1985). In Fig. 1, we plot the flux from a rocket experiment (Woods et al. 1994), divided by a factor of 100.

Tobiska (1991) and Tobiska & Eparvier (1998) have developed a different model, called EUV, using a more extended data base. In comparison to the previous ones, this model retrieves the solar flux from the decimetric index and its average. The latest versions use new input parameters computed from a previous version of the code (Tobiska et al. 2000). EUVAC (Richards et al. 1994) is based on a reference flux that differs from the one used by Torr and Hinteregger and that relies on a specific interpolation formula. EUVAC also adds physical constraints on the coronal flux. Its latest version, named HEUVAC (Richards et al. 2006), extends the EUV model below 5 nm and includes data from the SEE instrument onboard TIMED (Woods et al. 2005). All these models are reviewed in Lilensten et al. (2008).

The solid line in Fig. 1 represent typical EUV/XUV flux measured in the Earth atmosphere by a rocket experiment and divided by a factor of 100 to account for the distance from Saturn to the Sun. In the simulation, we used the semi-empirical model solar 2000 (Tobiska & Eparvier 1998). The total energy flux through this source is equal to 5.3×10^{10} eV cm^{-2} s^{-1}. (Integration done above 10 eV, if the visible is taken into account, the value grows up to 1.5×10^{16} eV cm^{-2} s^{-1}.)

2.2. The electron precipitation source

The considered electron precipitation spectrum plotted in Fig. 1 was taken from the measurements of the T5 fly-by (Cravens et al. 2009). It was measured by the Cassini electron spectrometer (CAPS ELS) (Coates et al. 2007; Cravens et al. 2009) from 0.6 eV to 28.250 keV (Young et al. 2004). These electrons come from the magnetosphere of Saturn and are embedded in the magnetic field draped around Titan (Modolo & Chanteur 2008; Cravens et al. 2009). In Cravens et al. (2009), the electron spectrum measured at 2700 km had to be divided by a factor of 10 to have the model fit the measurement correctly at an altitude of 1200 km. In Fig. 1, we did not divide the flux. A detailed study of this problem of division can be found in Part II, "Electron precipitation along magnetic field lines" The total energy flux through this source is equal to 2.3×10^9 eV cm^{-2} s^{-1}.

2.3. The proton and ion precipitation sources

There are several ions precipitating in Titan's atmosphere, coming from the magnetosphere of Saturn, as for the precipitating electrons. The largest is the proton source (Fig. 1). It is measured by the MIMI instrument onboard CASSINI (Krimigis et al. 2004) from 7 keV to 8 MeV. In the present study, we used the T5 flyby data to compare with the literature. However, the chemical study of this spectrum has not been published, so the ions cannot be distinguished. Following Cravens et al. (2008), we assume either that the whole flux is made of protons or of atomic oxygen ions. We used the spectrum of Cravens et al. (2008), which contains an interpolation of the spectrum down to 2 keV for the T5 conditions. The total energy flux through this source is equal to 1.0×10^9 eV cm^{-2} s^{-1}, if we take the strong conditions for the protons above 20 keV. If we take the lower energy protons, down to 2 keV, it gives 2.3×10^9 eV cm^{-2} s^{-1} (exactly as the electron precipitation). If we take the quiet condition with protons above 20 keV, however, it comes down to 9.9×10^7 eV cm^{-2} s^{-1}.

2.4. The cosmic ray source

The cosmic ray spectrum is based on the model of local interstellar spectrum (LIS) of Burger et al. (2000), corrected to fit the Titan conditions. This correction corresponds to a modulation that varies with the varying solar activity and is often described in terms of the so-called force-field model. The only explicit parameter of this model is the modulation potential whose value is given in units of MV (Usoskin 2005, and references herein).

We use a value of 300 MV at Titan, which corresponds to the 400 MV flux parameter at Earth, used in Molina-Cuberos et al. (1999b) as a solar minimum condition. This result is based on measurements by different probes. If we are in the inner heliosphere (out to >20 AU from the sun), we can consider with Webber (1987) a 10 MV variation of ϕ per AU. We therefore consider a maximum 1200 MV value for ϕ during high solar activity. The upper limit of our flux is set at 1 TeV. Above this energy limit, the cosmic ray cascade mainly reaches the ground and has very little influence into the atmosphere. The cosmic rays are mainly protons, with a low percentage of alpha and higher mass ions, which are neglected in the present study. This is a first approximation, because high-mass ions have a stronger influence than protons, and the increase in ion production can reach more than 50%, depending on the altitude (Velinov & Mateev 2008; Velinov 2008). This computation will be improved in the future. The total energy flux through this source, computed by integrating the precipitation spectrum between the cutoff and 1 TeV, is equal to 1.4×10^9 eV cm^{-2} s^{-1}.

2.5. The energy cut

Figure 2 shows the transmission probability of cosmic ray protons in the magnetosphere of Saturn at the position of Titan. The transmission probability was evaluated with the planetocosmic code and the Acuna et al. (1983) model of Saturn's internal source of the magnetic field. Based on the results shown in Fig. 2, we assumed a rigidity cutoff of 0.2 GV, which means an energy cutoff of 20 MeV for cosmic ray protons. (The relativistic formula between the kinetic energy E_k and the rigidity R is,

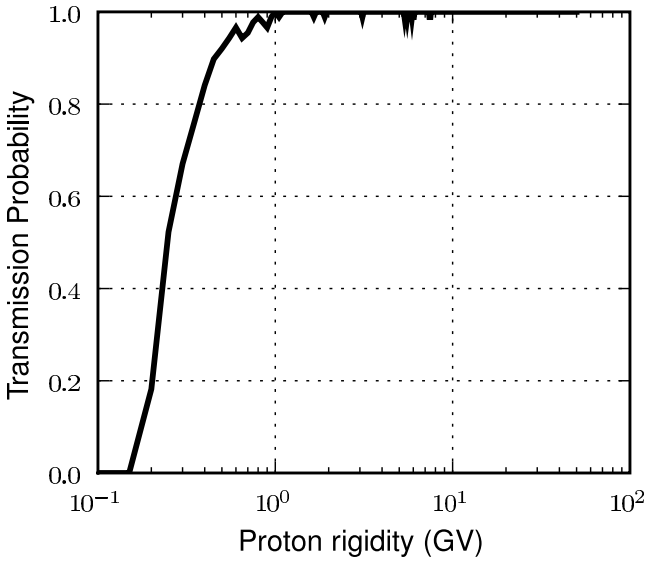

Fig. 2. Transmission probability of cosmic ray protons into the magnetosphere of Saturn at the position of Titan.

considering the mass M of the particle, each one in units of GeV: $E_k = \sqrt{M^2 + R^2} - M$.)

3. Method

We computed the ionization in the Titan's atmosphere, using the transTitan model coupled with the planetocosmics Geant4 code for taking the contribution of cosmic rays into account.

3.1. The transTitan model

In the past years, we have developed a family code whose generic name is Trans*. It has been adapted to several planets, becoming successively transsolo (Lummerzheim & Lilensten 1994), transcar (Lilensten & Blelly 2002), tran4 (Simon et al. 2007) in the case of Earth, and, for orther planets, transTitan (Lilensten et al. 2005a,b), transMars (Witasse et al. 2003, 2002; Simon et al. 2008), transVenus (Gronoff et al. 2007, 2008). The transTitan code used here consists of primary production through photoabsorption and secondary production through electron impacts. The primary production is computed through a Beer-Lambert law, and the secondary production computation requires solving a kinetic transport equation. The neutral atmosphere is described in Müller-Wodarg et al. (2000), where only N_2 and CH_4 species are taken into account. The exospheric temperature is 175 K. The altitude range covered by our computation is 600 km to 1600 km. The photon absorption cross sections come from Torr & Torr (1985) and Fennelly & Torr (1992) for N_2 and from Samson et al. (1989) for CH_4.

3.2. The planetocosmics model

The PLANETOCOSMICS code (`http://cosray.unibe.ch/~laurent/planetocosmics`) is a Geant4 application originally designed to compute the electromagnetic and hadronic interaction of energetic particles (<1 TeV) with the Earth, Mars and Mercury, taking the respective planetary atmosphere, magnetic field, and soil into account (Desorgher et al. 2005; Bütikofer et al. 2008). The code was developed so that the implementation of new atmospheric and magnetic field models, as well as the extension to other planetary environments, is rather simple. For this study PLANETOCOSMICS was adapted to the Titan/Saturn magnetic and atmospheric environment as described in Sects. 2.5 and 3.1.

3.3. Coupling the two models

In planetocosmics, the cosmic rays impact the neutral atmosphere to create a cascade of particles. There are energetic electrons within these particles. Many of the particles in the cascade are able to create secondary ionization. To compute this secondary production, planetocosmic computes the energy deposition at each altitude in the atmosphere, which, in the coupled model, is divided by a value of 35 eV per ion-electron pair creation. This method is fast and easy to implement. However, it does not allow computing the secondary ion production, and for some applications it may not be accurate enough. The value of 35 eV per ion-electron pair creation was checked in the lower atmosphere of Titan by using the TransTitan code below 100 km altitude with standard fluxes. We used the flux of energetic electrons produced by cosmic impact on the atmosphere as a source in the kinetic code. This primary source is called "primary cosmoelectron source". It degrades its energy through collisions to create ionization, dissociation, excitation, and heating as described in the Boltzmann equation. This coupling therefore allows computing many more parameters than the simple use of 35 eV per pair. Unfortunately, the energetic electrons are not the only particles created in the cascade. They represent only 10% of the total energy scattered. For the other 90%, it is still necessary to use the 35 eV per pair to describe the energy deposition.

4. Results

4.1. Ionization due to the UV-EUV flux

The ionization due to electromagnetic solar flux has been widely studied in Lilensten et al. (2005b,a), which takes both primary and secondary productions into account. There is no difference between this study and the present one. The main results are shown in Fig. 3 for a solar zenith angle of 40 ° and a solar activity decimetric index ($F_{10.7}$) of 80. It results in an electron production that maximizes at 1000 km with a value of about 10 $cm^{-3}\ s^{-1}$. The major ions are N_2^+, N^+, CH_4^+, and CH_3^+. There is no influence from the EUV–XUV flux below an altitude of about 700 km. Both the production and the density profiles exhibit two layers that are comparable to the Earth shapes and therefore have been nicknamed F and E regions (Galand et al. 1999).

4.2. Ionization from precipitating electrons

The electron impact ionization is computed with transTitan, and can be seen in Fig. 6. The input flux in transTitan is directly the flux in Fig. 1. The transport code allows computation of the different ion productions. The main ions are the same as for the EUV production. However, the cross sections are not very well known for impact of high-energy electrons on CH_4. Following (Straub et al. 1997; Luna et al. 2003), we used a branching ratio of 50% for CH_4^+ and 50% for the other ions. For a 1 keV electrons, the other ions are CH_3^+ (69.7%), CH_2^+ (11%), CH^+ (4.7%),C^+ (1.4%), H_2^+ (0.9%), and H^+ (12.3%).

In Fig. 4, we show the ionization due to precipitating electrons with different characteristic energies as computed by planetocosmics. We computed the production due to isotropic, mono-energetic electron input fluxes. With energies ranging

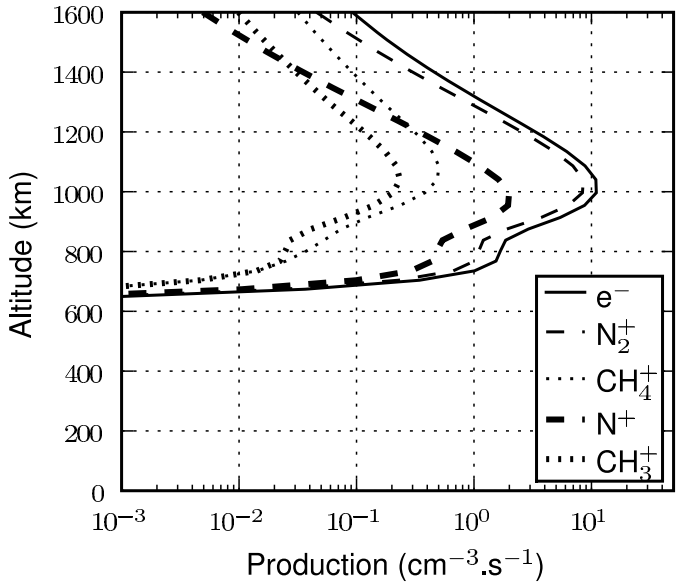

Fig. 3. Ionization due to EUV/XUV solar flux computed for a solar zenith angle of 40° with a solar flux given by $F_{10.7} = 80$.

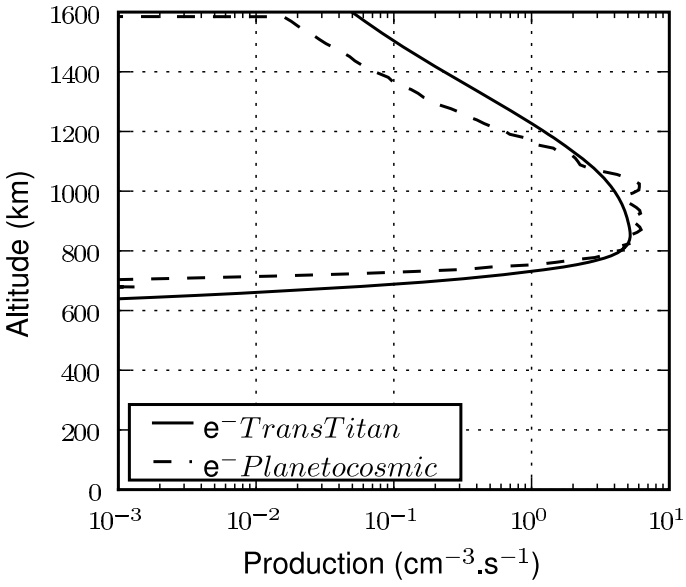

Fig. 5. Comparison of electron impact ionization computed with transTitan and planetocosmics.

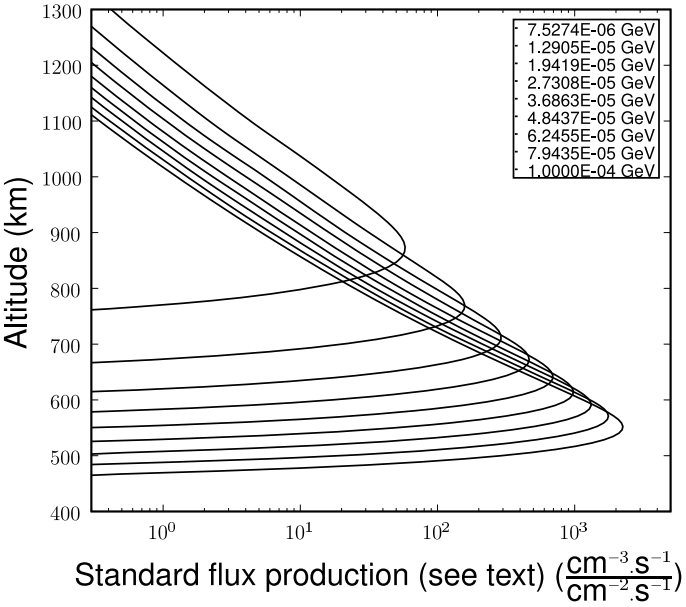

Fig. 4. Ionization from mono-energetic electrons, with an isotropic distribution computed with planetocosmics. The higher in altitude the peak, the less energetic the electrons. The aim of this figure is to show the peak altitude with respect to the energy. In the following, the electron influence is computed through TransTitan, which is more accurate and is able to discriminate between the ionized species.

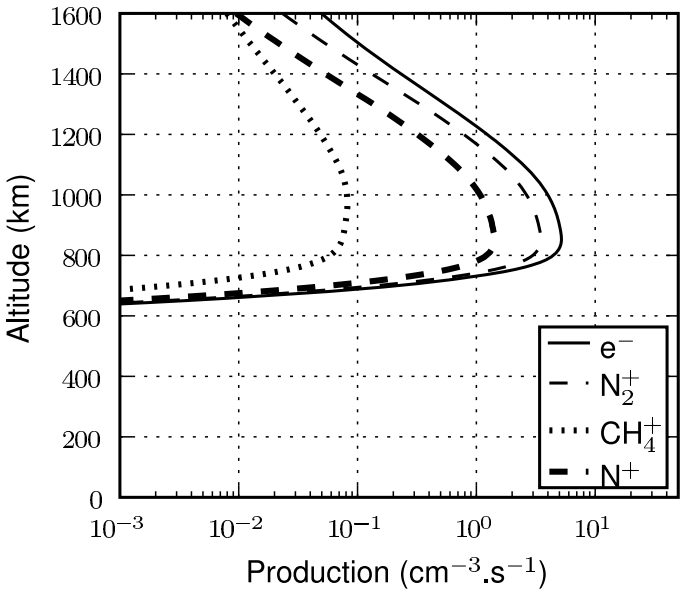

Fig. 6. Electron impact ionization computed with the Cassini T5's flyby electron flux conditions with transTitan. A vertical magnetic flux line is considered.

from 1 keV up to 100 keV (not all profiles shown in the figure). The production was computed on an average based on more than 3000 runs on each angle. The same numerical mode was used with planetocosmics all through this study. The electrons typically ionize above 550 km. The 100 keV electrons produce a maximum at 550 km and the 1 keV electrons at 900 km. The amplitudes of production on this plot cannot be interpreted directly. They correspond to a production for an input flux of 1 electron cm^{-2} s^{-1} on top of the ionosphere (and are therefore in unit of (cm^{-3} s^{-1})/(cm^{-2} s^{-1}). To be interpreted in term of production, this value has to be multiplied by the input spectrum from Fig. 1 and integrated over the energy range. This is shown in Fig. 5. The electron production due to the electron precipitated flux peaks at 900 km below the EUV–XUV peak. The amplitude of production is about 5 cm^{-3} s^{-1}. We compared this computation with the results of the full transport equation solution, shown in the same figure, and the values compare very well. The accuracy is better above about 1100 km with the transport code, because the production at high altitude stem from to low energy fluxes that are not taken into account in planetocosmics. One of the reasons is that the 35 eV value per creation of ion electron pair goes wrong below these energies.

4.3. Ionization from precipitating protons

In Fig. 7, we present the ionization from precipitating protons with different characteristic energies. The set in energy has been

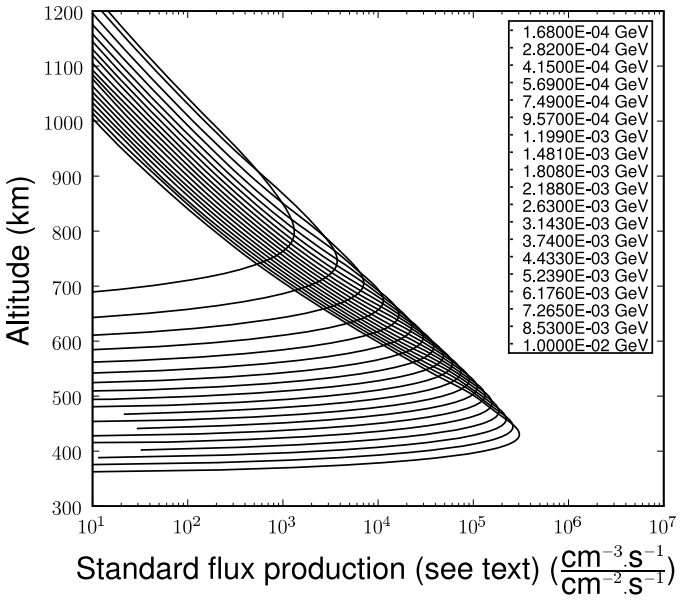

Fig. 7. Ionization from mono-energetic protons, with an isotropic distribution computed with planetocosmics. The higher in altitude the peak, the less energetic the protons.

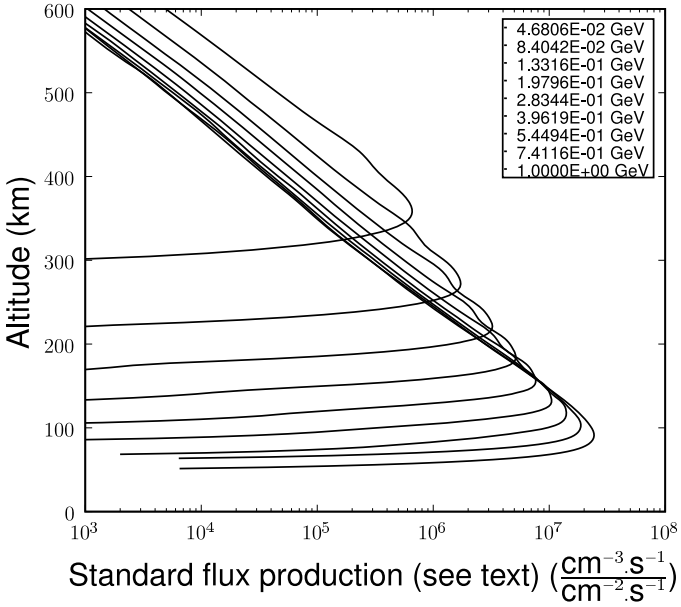

Fig. 8. Ionization due to mono-energetic isotropically distributed protons, with energy near the cutoff, computed with planetocosmics. The higher in altitude the peak, the less energetic the protons.

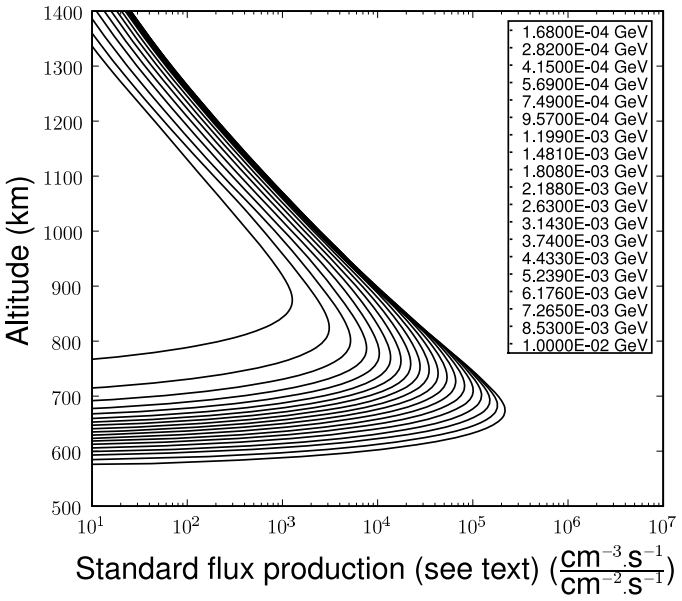

Fig. 9. Ionization due to mono-energetic atomic oxygen ions O^+, with an isotropic distribution computed with planetocosmics. The higher in altitude the peak, the less energetic the ions.

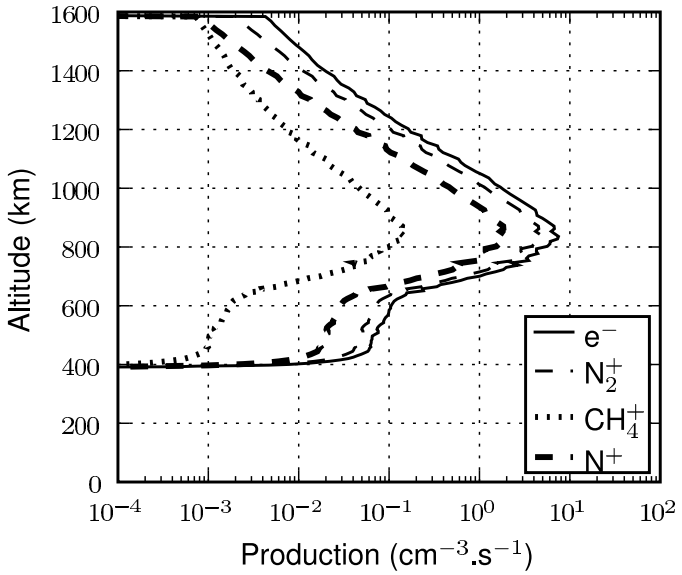

Fig. 10. Ionization due to precipitating protons for the T5 (active) conditions, computed with the coupled model.

reduced to fit the energy detection range of the Cassini probe. While in Fig. 8, we plot the influence of the protons in the 10 MeV–1 GeV range, in such energies we are at the limit between the protons accelerated in the magnetosphere of Saturn and the cosmic rays. In these figures, the secondary electrons (produced by proton-ionization) are taken into account as an energy deposition at the altitude where they are produced, whereas in the coupled code, the electrons are introduced into the kinetic part.

The interesting point is that the protons with energy above 1 MeV have an ion production peak below 500 km. In Fig. 11, the ion production from proton precipitations is presented for quiet conditions. The production peak is close to 750 km with an amplitude of 0.3 $cm^{-3}\,s^{-1}$. The T5 conditions (Fig. 10) corresponds to active conditions of protons; the peak is close to 850 km with an amplitude of 6 $cm^{-3}\,s^{-1}$. In these two plots, a secondary layer shows up between 400 km and 600 km, with an amplitude slightly smaller than 0.1 $cm^{-3}\,s^{-1}$. It originates in the precipitations of protons with energies above 1 MeV as shown in Fig. 7.

The influence can be seen in Fig. 9 for oxygen. In this figure, the secondary electrons are taken into account as an energy deposition at the altitude where they are produced, whereas in the coupled code, the electrons are introduced into the kinetic part. At equal energy, the oxygen ions have an influence at higher altitude. This kind of precipitation cannot create an ion layer below 600 km. In Fig. 12, we present the ion production due to precipitating oxygen ions. Following Cravens et al. (2008), we

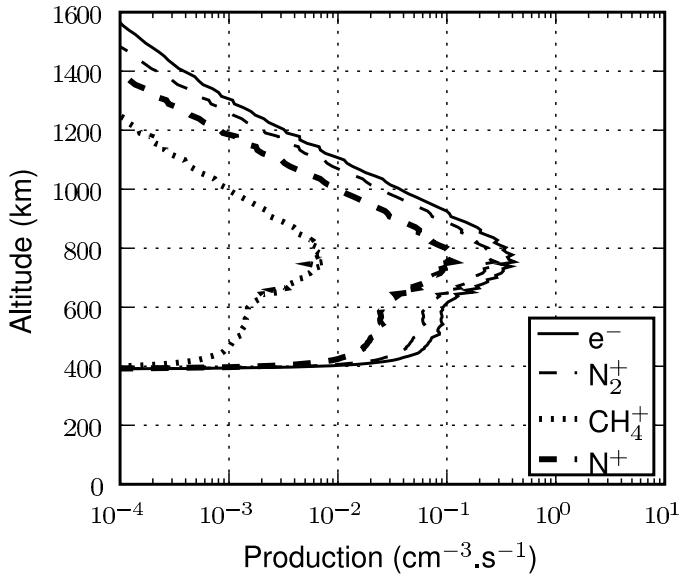

Fig. 11. Ionization due to precipitating protons for quiet conditions.

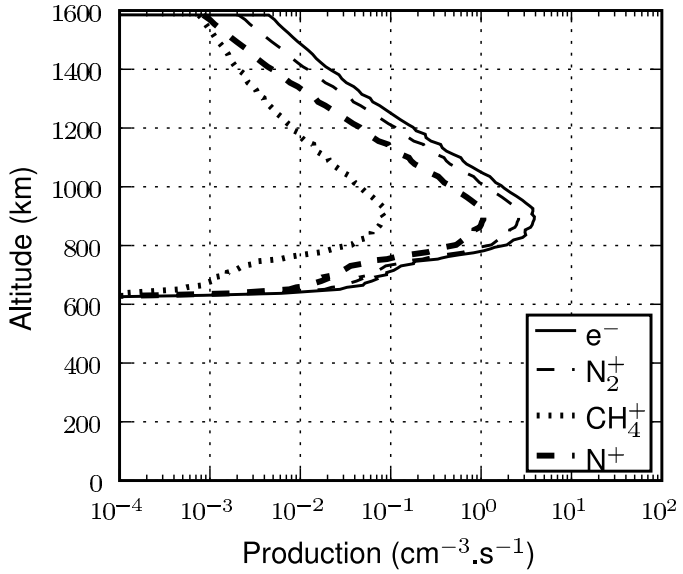

Fig. 12. Ionization due to oxygen (O^+) precipitation (the T5 protons spectrum is considered as oxygen here).

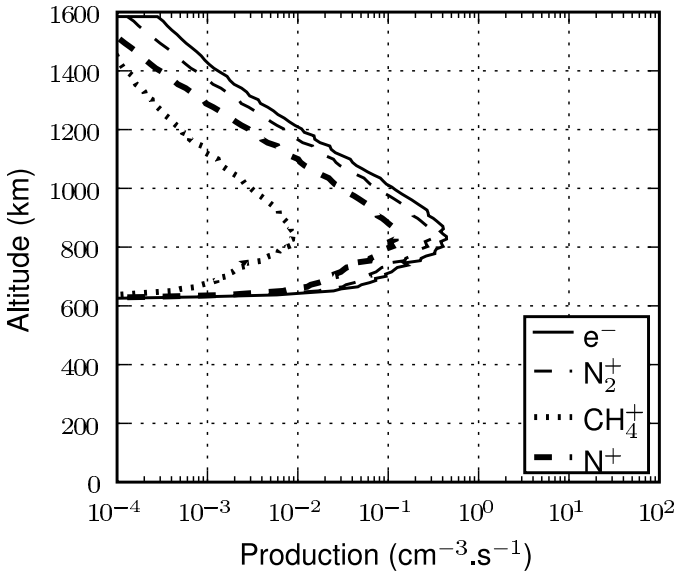

Fig. 13. Ionization due to oxygen (O^+) precipitation with the low energy protons spectrum considered as oxygen.

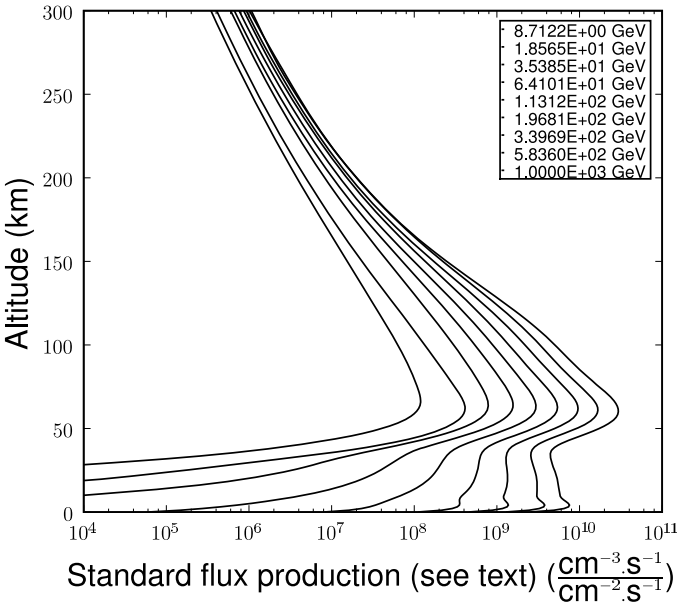

Fig. 14. Ionization due to mono-energetic cosmic ray protons, with an isotropic distribution computed with Planetocosmics. The higher in altitude the peak is, the less energetic the cosmic ray are.

assume for this numerical study that the whole T5 precipitation spectrum is made of O^+. The peak is close to 900 km with an amplitude of 3 cm^{-3} s^{-1}. For quiet conditions, (Fig. 13) the peak is at 850 km with an amplitude of 0.4 cm^{-3} s^{-1}. In the case of ion oxygen precipitations, there is no secondary layer below the peak.

4.4. Ionization due to the cosmic rays

In Fig. 14, we present the influence of cosmic rays in the GeV–TeV range. In this figure, the secondary electrons are taken into account as an energy deposition at the altitude where they are produced, whereas in the coupled code, the electrons are introduced into the kinetic part. The maximum ion production is always near 65 km, but the shape below is modified, because of the cascade of particles. Figure 15 shows the influence of galactic cosmic rays below 600 km down to the ground. Figure 16 shows a zoom of the production at low altitude. The ion production peak is at 65 km with an amplitude of 15 cm^{-3} s^{-1}. Below the peak, the production due to the cascade down to the ground is clearly visible. In Fig. 17, we compare the result for low solar activity (350 MV) with highest solar activity (1200 MV). During low solar activity, the solar modulation parameter is lower, the cosmic ray flux is higher, and therefore the production. For both extreme of solar activity, the maximum ion production peak is at 65 km. But the peak for high solar activity has a smaller amplitude of 9 cm^{-3} s^{-1}.

4.5. Total ionization in the atmosphere of Titan

Considering the different particle precipitation, we plotted the whole ionization in a single figure. We considered it for the T5 Cassini flyby conditions, which occurred during the night.

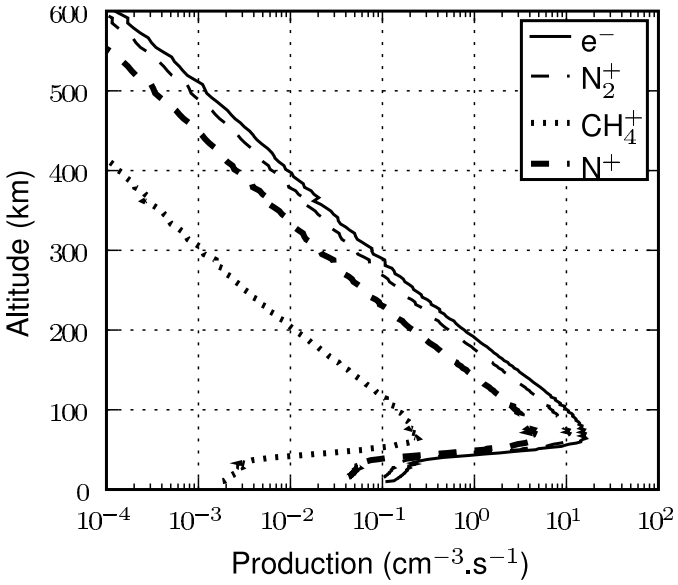

Fig. 15. Ionization due to galactic cosmic rays computed with the coupled model.

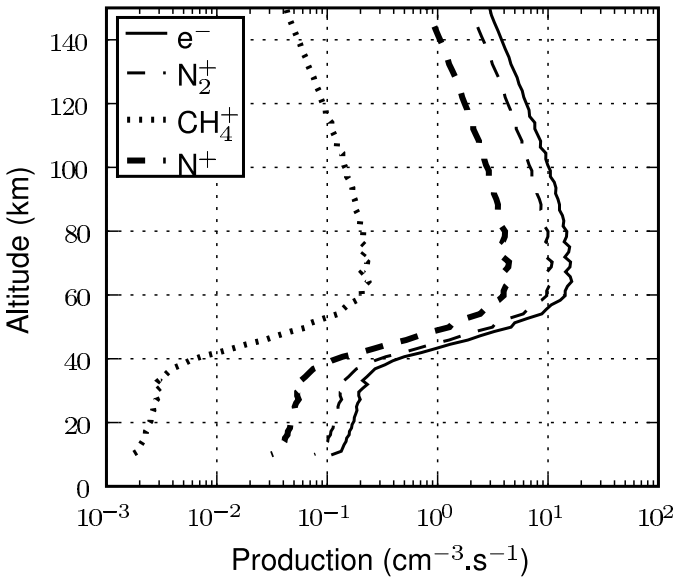

Fig. 16. Zoom on the ionization due to galactic cosmic rays at low altitude.

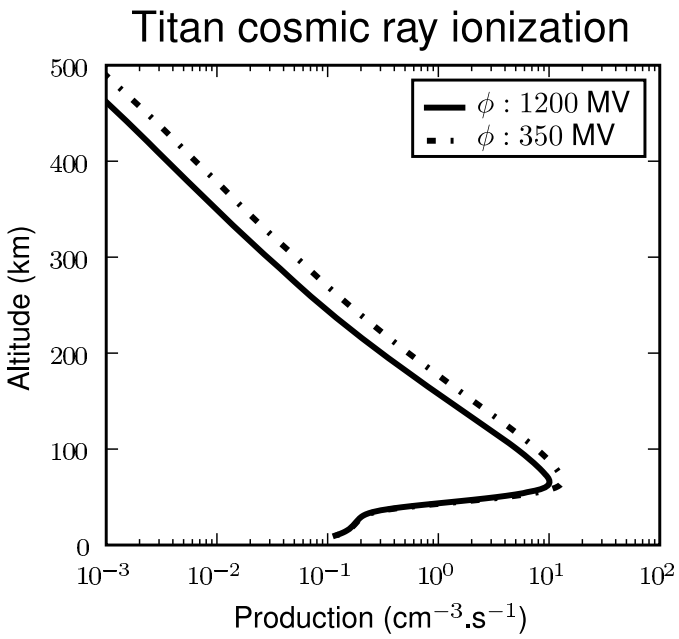

Fig. 17. Influence of the solar activity on the cosmic ray production.

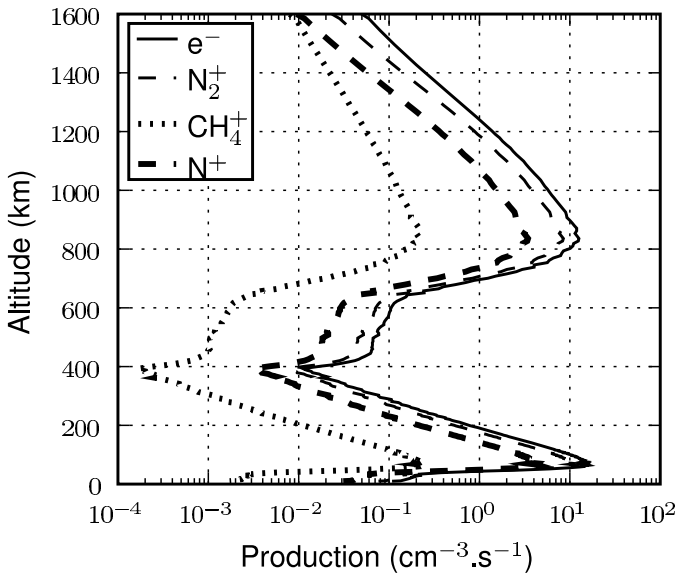

Fig. 18. Total ionization computed for the nightside T5 flyby conditions.

Therefore, electrons, protons, and cosmic rays are taken into account in Fig. 18. The interesting point is that the peak value of electron (photons for the dayside conditions) and cosmic ray ionization are very similar. Considering that the high energy protons have a strong influence near 500 km, we can consider that Titan has three main ionization layers.

5. Discussion

5.1. Comparison with other models

The cosmic ray impact has been computed with a different technique by Molina-Cuberos et al. (1999b), Capone et al. (1976, 1980), Borucki et al. (1987, 2006), Borucki & Whitten (2008). Their approach solves a Boltzmann kinetic transport equation where the redistribution function is written such that the numbers of particles in the cascade are well reproduced (O'Brien 1969). The results are very close to the present study, with an ion production rate maximizing at 65 km (Molina-Cuberos et al. 1999b) and a production of 10 cm^{-3} s^{-1}. Comparing with other works based on the same Boltzmann approach Borucki & Whitten (2008) and Lavvas et al. (2008a), some minor differences appear depending on the neutral atmosphere and the solar activity. In Lavvas et al. (2008a,b), the peak altitude is equal to 100 km but (as in Molina-Cuberos et al. 1999a; Borucki & Whitten 2008) a chemistry code is then used to reproduce the densities.

The proton impact has been studied by Borucki et al. (1987) and Cravens et al. (2008). Comparing to our results, the proton ionization peak is lower in Borucki et al. (1987), at 600 km and more intense: 10. cm^{-3} s^{-1}. The difference comes mainly from the difference in the precipitation spectrum, then from the use of an unidirectional flux in Borucki et al. (1987), with the use of the Banks & Kockart (1973) technique. In Cravens et al. (2008), the peak is at 750 km and the amplitude of N_2^+ production

value is the same as this work 0.3 $cm^{-3}\,s^{-1}$ for quiet conditions. Moreover, the production of this work is slightly lower at 500 km, but the secondary layer is more visible. The difference comes mainly from the unidirectional proton flux hypothesis used in Cravens et al. (2008). For active conditions, the results for oxygen ions are practically the same between this work and Cravens et al. (2008) with a peak production of N_2^+ of 2. $cm^{-3}\,s^{-1}$ at 900 km.

The electron impact has been studied in Agren et al. (2007), and re-analyzed in Cravens et al. (2008, 2009), with an updated precipitation flux (used in this work). In order to fit the flux measurements at 1200 km with the model using a precipitation flux measured at 2730 km, the authors had to divide by 10 the input flux. Thanks to that work, an N_2^+ production peak is computed at 950 km with an amplitude of 0.4 $cm^{-3}\,s^{-1}$. With the same flux, our model computes a N_2^+ production peak at 850 km with an amplitude of 0.3 $cm^{-3}\,s^{-1}$ (basically, the same production as in Fig. 6, but divided by 10). The problem of the differences between the model and the measurement at 1200 km our model, which considers isotropic precipitation along the vertical axis, shows the same need for dividing the flux by 10. This problem should be resolved by considering that the precipitation is not vertical, but instead follows a magnetic field line which can have a complex shape (see, for example Modolo et al. 2007; Modolo & Chanteur 2008). A deeper analysis of the precipitation along the magnetic field lines in Titan can be found in part II "Electron precipitation along magnetic field lines".

5.2. Full height profile and comparison with data

The Huygens experiment found an ionized layer at 65 km, which corresponds to the production peak in Fig. 16 (López-Moreno et al. 2008; Hamelin et al. 2007).

The radio experiment onboard Cassini allowed retrieval of the ion densities down to 200 km (Kliore et al. 2008). Computing the ion densities from the ion production necessitates a full chemistry code, which is not available in the present work. We aim at establishing a full profile of the ion production from the bottom of the atmosphere to the top of the ionosphere; however, some simple comparisons can still be made. When an ion is largely preponderant, or when the ion profile is made of a mixture of ions with approximately constant abundances, it is possible to reduce the chemistry to a single reaction with a chemical coefficient called an effective coefficient rate $\alpha_{\rm eff}$ (Banks & Kockart 1973). This coefficient varies with altitude. In Galand et al. (1999), this method is successfully compared to a full chemistry code for the electron density profile above 900 km. It is also used in Cravens et al. (2008). In that case, the electron density is simply proportional to the square root of the electron production (this does not apply of course for the ions separately): $n_{\rm e} = \sqrt{P_{\rm e}/\alpha_{\rm eff}}$ (where $n_{\rm e}$ is the electron density and $P_{\rm e}$ the electron production). This simple method neglects the diffusion, which is negligible at low altitudes. However, it allows comparison of the shapes of the computed electron productions to the measured electron densities. In Fig. 18, we plot the full electron and ion profile for T5 conditions. This shows for the first time an integrated computation from 0 to 1600 km due to three different sources with a coupling through the secondary electron transport. Although this curve cannot be compared in terms of intensity to the nightside measured electron density profiles published in Kliore et al. (2008) (because the effective coefficient rate varies with altitude), the global shape can still be compared. At night, the measurements show a layer around about

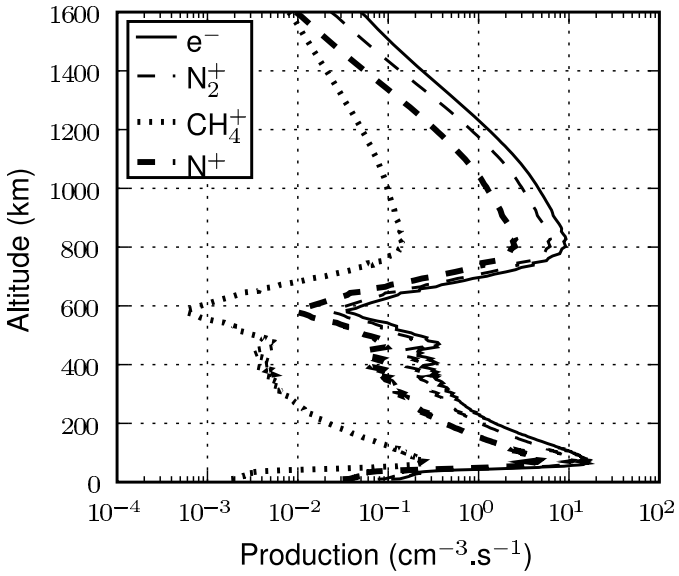

Fig. 19. Complete T5 simulation, as in Fig.18 with the interpolation of the spectrum.

500 km. This layer originates in our analysis in the precipitation of about 1 MeV protons and corresponds to the secondary layer in Fig. 10.

Another feature of the measured profiles is an increase in the density at the bottom of the measurement, i.e. below about 400 km. This clearly comes from the cosmic rays in our analysis. In the spectrum of precipitating protons (Fig. 1), there are missing points above 4 MeV and the point where this precipitation flux should join the cosmic ray flux. Indeed, the proton flux is much higher than the cosmic ray one at these energies, and the effect of this gap on the profile could be strong. The shape of precipitations filling this gap is still unknown. To approach this question, we filled it with a linear interpolation between 4 MeV and 0.1 GeV and computed the resulting electron production profile. The results are shown in Fig. 19. The secondary layer between 600 and 400 km disappears. This does not compare to the measured electron density profiles (although these measurements are above 200 km). Therefore, we conclude that the gap between 4 MeV and 0.1 GeV is physical and that there is no continuity in the spectrum because the sources are different. The exact location of the gap still remains unknown and cannot be deduced from the current set of electron density observations.

5.3. Reproducing data

We study the conditions of the T14 fly-by of Cassini in detail as described in Kliore et al. (2008). Because we did not have particle precipitation fluxes, we tried to reproduce them from the data. We fit the electron density computed as described above to the one measured by Cassini to deduce the particle precipitation fluxes. Because the data are coming from radio occultation, the solar zenith angle (SZA) is large (close to 90°), here, the model fits the data with an SZA of 99°. The secondary layer, at 1000 km is explained by photoionization and electron precipitation ($\alpha_{\rm eff} = 3 \times 10^{-7}$ $cm^3\,s^{-1}$). The electron precipitation spectrum is equal to the $T5$ one divided by 50. To fit the proton layer, at 500 km, we inverted the data with the same α coefficient. The proton precipitation spectrum deduced from this work can be seen in Fig. 20. By comparison with previous data, we can estimate that both our precipitation flux and the α factor

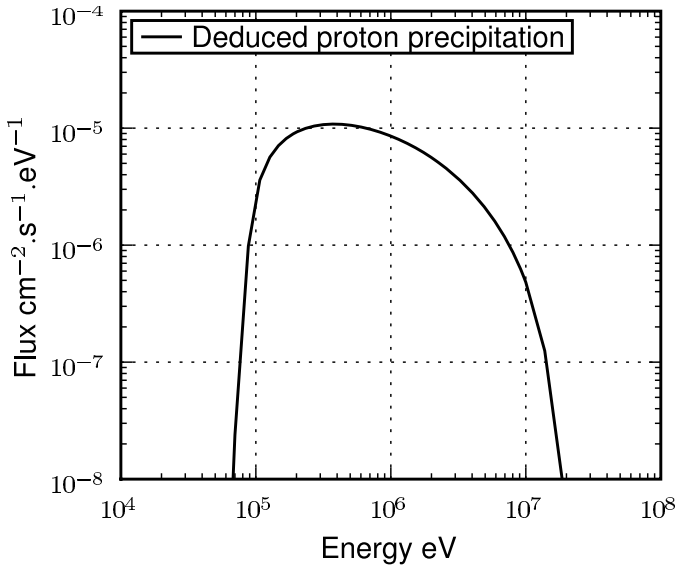

Fig. 20. Proton precipitation used for the comparison with data in Fig. 21.

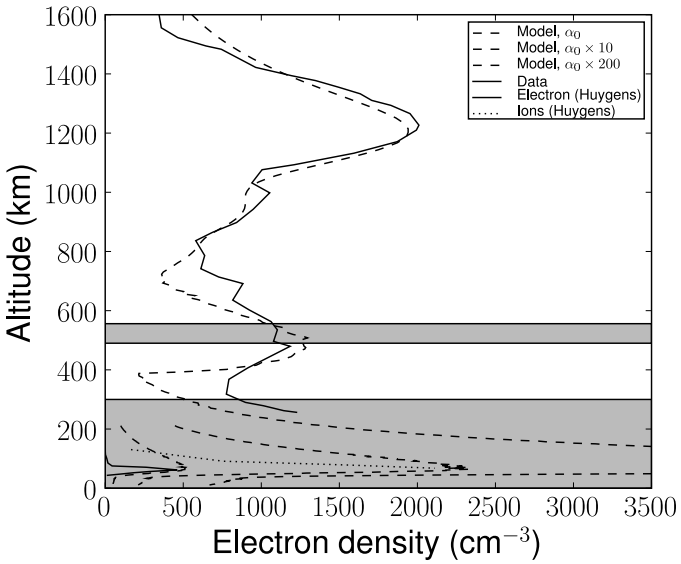

Fig. 21. Interpretation of the complete Titan electron density with different input sources. Electron density data above 300 km comes from Kliore et al. (2008), ion and electron densities below 100 km come from López-Moreno et al. (2008). The position of the haze layers is highlighted in gray.

at these altitudes are underestimated. At low altitudes, we used the López-Moreno et al. (2008) data for electron and ion density detected by Huygens. To approximate the ion and the electron peaks, we used an $\alpha_{\rm eff}$ if 5×10^{-5} cm^3 s^{-1}. The shape is not reproduced exactly, because of a more complex chemistry (Borucki & Whitten 2008). The result of this inversion and the comparison with the data can be seen in Fig. 21. To compare it with the physical properties of the atmosphere of Titan, we highlighted the position of the main (0–300 km) and detached (450 km) haze layers (Rannou et al. 2002; Lavvas et al. 2009). These layers are at the altitude of cosmic ray and proton production peak, suggesting that these precipitation are at the origin of the haze creation.

6. Conclusion

For the first time, a full electron and ion production profile has been computed with an integrated code from 0 to 1600 km. It considers the solar EUV–XUV flux, the electrons, and protons of different origins (solar and magnetospheric), the oxygen ions, and finally the cosmic rays as sources. It is based on coupling different approaches.

This profile compares qualitatively very well to Cassini-Huygens measurements and to other publications for the different sources separately. It allows the effect of the different input sources to be distinguished and the shape of the precipitations to be deduced for a given electron profile. The next step is to include the computed electron and ion production in a chemistry/dynamics code in order to understand the origin of the large hydrocarbon molecules found in Titan's atmosphere. The correlation between the position of the main haze layer and the detached haze layer respectively with the cosmic ray production peak and the proton production peak effectively suggests that the haze may be created by the ions resulting from the precipitation of these particles.

Acknowledgements. The authors thank Mathieu Barthelemy (LPG, France), Roland Thissen (LPG, France), Véronique Vuitton (LPG, France) and Cyril Simon, (BIRA, Belgique) for useful discussions. The planetocosmics simulation were made using the CIGRI system on the CIMENT platform in Grenoble (France). We thank Bruno Bzeznik (IMAG, France) for teaching us this system, and his useful advice. Work at the University of Bern was supported by the Swiss National Science Foundation (grant 200020/113704) and by the Swiss State Secretariat for Education and Research (grant COST-724/C05.0034).

References

Acuna, M. H., Connerney, J. E. P., & Ness, N. F. 1983, J. Geophys. Res., 88, 8771
Agren, K., Wahlund, J. E., Modolo, R., et al. 2007, Annales Geophysicae, 25, 2359
Banks, & Kockart 1973, Aeronomy, ed. A. Press
Borucki, W. J., & Whitten, R. C. 2008, Planet. Space Sci., 56, 19
Borucki, W. J., Levin, Z., Whitten, R. C., et al. 1987, Icarus, 72, 604
Borucki, W. J., Whitten, R. C., Bakes, E. L. O., Barth, E., & Tripathi, S. 2006, Icarus, 181, 527
Burger, R. A., Potgieter, M. S., & Heber, B. 2000, J. Geophys. Res., 105, 27447
Bütikofer, R., Flückiger, E. O., Desorgher, L., & Moser, M. R. 2008, Sci. Total Environ., 391, 177
Capone, L. A., Whitten, R. C., Dubach, J., Prasad, S. S., & Huntress, Jr., W. T. 1976, Icarus, 28, 367
Capone, L. A., Dubach, J., Whitten, R. C., Prasad, S. S., & Santhanam, K. 1980, Icarus, 44, 72
Coates, A. J., Crary, F. J., Young, D. T., et al. 2007, Geophys. Res. Lett., 34
Cravens, T. E., Robertson, I. P., Ledvina, S. A., et al. 2008, Geophys. Res. Lett., 35
Cravens, T. E., Robertson, I. P., Waite, J. H., et al. 2009, Icarus, 199, 174
Desorgher, L., Flückiger, E. O., Gurtner, M., Moser, M. R., & Bütikofer, R. 2005, Int. J. Modern Phys. A, 20, 6802
Fennelly, J. A., & Torr, D. G. 1992, Atomic Data and Nuclear Data Tables, 51, 321
Galand, M., Lilensten, J., Toublanc, D., & Maurice, S. 1999, Icarus, 140, 92
Gronoff, G., Lilensten, J., Simon, C., et al. 2007, A&A, 465, 641
Gronoff, G., Lilensten, J., Simon, C., et al. 2008, A&A, 482, 1015
G. Gronoff, J. Lilensten, & R. Modolo, A&A, 506, 965 (Paper II)
Hamelin, M., Béghin, C., Grard, R., et al. 2007, Planet. Space Sci., 55, 1964
Hinteregger, H. E. 1981, Adv. Sp. Res., 1, 39
Hinteregger, H. E., Bedo, D. E., & Manson, J. E. 1973, Radio Science, 8, 349
Hinteregger, H. E., Fukui, K., & Gilson, B. R. 1981, Geophys. Res. Lett., 8, 1147
Kliore, A. J., Nagy, A. F., Marouf, E. A., et al. 2008, J. Geophys. Res., 113
Krimigis, S. M., Mitchell, D. G., Hamilton, D. C., et al. 2004, Space Sci. Rev., 114, 233
Lavvas, P. P., Coustenis, A., & Vardavas, I. M. 2008a, Planet. Space Sci., 56, 27
Lavvas, P. P., Coustenis, A., & Vardavas, I. M. 2008b, Planet. Space Sci., 56, 67
Lavvas, P., Yelle, R., & Vuitton, V. 2009, Icarus, 201, 626
Lilensten, J., & Blelly, P. L. 2002, J. Atmospheric and Terrestrial Physics, 64, 775

Lilensten, J., Simon, C., Witasse, O., et al. 2005a, Icarus, 174, 285
Lilensten, J., Witasse, O., Simon, C., et al. 2005b, Geophys. Res. Lett., 32
Lilensten, J., Dudok de Wit, T., Kretzschmar, M., et al. 2008, Annales Geophysicae, 26, 269
López-Moreno, J. J., Molina-Cuberos, G. J., Hamelin, M., et al. 2008, Geophys. Res. Lett., 35
Lummerzheim, D., & Lilensten, J. 1994, Annales Geophysicae, 12, 1039
Luna, H., Cavalcanti, E. G., Nickles, J., Sigaud, G. M., & Montenegro, E. C. 2003, J. Phys. B: At. Mol. Opt. Phys., 36, 4717
Modolo, R., & Chanteur, G. M. 2008, J. Geophys. Res., 113
Modolo, R., Wahlund, J.-E., Boström, R., et al. 2007, Geophys. Res. Lett., 34
Molina-Cuberos, G. J., López-Moreno, J. J., Rodrigo, R., & Lara, L. M. 1999a, J. Geophys. Res., 104, 21997
Molina-Cuberos, G. J., López-Moreno, J. J., Rodrigo, R., Lara, L. M., & O'Brien, K. 1999b, Planet. Space Sci., 47, 1347
Müller-Wodarg, I. C. F., Yelle, R. V., Mendillo, M., Young, L. A., & Aylward, A. D. 2000, J. Geophys. Res., 105, 20833
O'Brien, K. 1969, Nucl. Instrum. Meth., 72, 93
Rannou, P., Hourdin, F., & McKay, C. P. 2002, Nature, 418, 853
Richards, P. G., Fennelly, J. A., & Torr, D. G. 1994, J. Geophys. Res., 99, 8981
Richards, P. G., Woods, T. N., & Peterson, W. K. 2006, Adv. Sp. Res., 37, 315
Samson, J. A. R., Haddad, G. N., Masuoka, T., Pareek, P. N., & Kilcoyne, D. A. L. 1989, J. Chem. Phys., 90, 6925
Simon, C., Lilensten, J., Moen, J., et al. 2007, Annales Geophysicae, 25, 661
Simon, C., Witasse, O., Leblanc, F., Gronoff, G., & Bertaux, J.-L. 2008, Planetary and Space Science
Straub, H. C., Lin, D., Lindsay, B. G., Smith, K. A., & Stebbings, R. F. 1997, J. Chem. Phys., 106, 4430
Tobiska, W. K. 1991, J. Atmosph. Terrestr. Phys., 53, 1005
Tobiska, W. K., & Eparvier, F. G. 1998, Sol. Phys., 177, 147
Tobiska, W. K., Woods, T., Eparvier, F., et al. 2000, J. Atmosph. and Solar-Terrestr. Phys., 62, 1233
Torr, M. R., & Torr, D. G. 1985, J. Geophys. Res., 90, 6675
Torr, M. R., Torr, D. G., Ong, R. A., & Hinteregger, H. E. 1979, Geophys. Res. Lett., 6, 771
Usoskin, I. G. 2005, J. Geophys. Res., 110, A12108
Velinov, P. 2008, J. Atmospher. Solar-Terrestr. Phys., 70, 574
Velinov, P. I. Y., & Mateev, L. 2008, Adv. Space Res., 42, 1586
Webber, W. R. 1987, A&A, 179, 277
Witasse, O., Dutuit, O., Lilensten, J., et al. 2002, Geophys. Res. Lett., 29, 104
Witasse, O., Dutuit, O., Lilensten, J., et al. 2003, Geophys. Res. Lett., 30, 12
Woods, T. N., Rottman, G. J., Bailey, S. M., & Solomon, S. C. 1994, Opt. Eng., 33, 438
Woods, T. N., Eparvier, F. G., Bailey, S. M., et al. 2005, J. Geophys. Res., 110
Young, D. T., Berthelier, J. J., Blanc, M., et al. 2004, Space Sci. Rev., 114, 1